

**Infrared enhancement in single-baryon systems**Songlin Lv<sup>1</sup> and Bingwei Long<sup>1,\*</sup>*<sup>1</sup>Center for Theoretical Physics, Department of Physics,  
Sichuan University, 29 Wang-Jiang Road, Chengdu, Sichuan 610064, China*

(Dated: May 22, 2016)

**Abstract**

The pion-baryon triangle diagram is inspected for the special kinematic region in which the squared momentum transfer is close to  $4m_\pi^2$ . The pion propagators can have very small energies, as opposed to  $\sim m_\pi$  in the physical region, which allows the nucleon propagator to be near its mass shell. This observation leads us to conclude that in this particular domain the triangle diagram is augmented by  $\mathcal{O}(m_N/m_\pi)$  compared with the standard counting of chiral perturbation theory, hence an infrared enhancement in the single-baryon sector.

---

\*Electronic address: bingwei@scu.edu.cn

## I. INTRODUCTION

As far as one-baryon processes are concerned, baryons have always been approximated as static objects at leading order in heavy-baryon chiral perturbation theory (HBChPT), and recoil corrections are treated as subleading perturbations [1]. However, the phenomenological successes of covariant approaches, in which recoil corrections are in effect resummed to all orders, challenged this point of view [2–11]. The initial theoretical rationale for covariant treatment of baryons comes from Ref. [2] (also touched upon in Refs. [12, 13]), in which the pion-baryon triangle diagram was examined. Figure 1 shows the said diagram, where  $p$  is the incoming 4-momentum of the baryon and  $q$  the momentum transfer. With different vertexes, this diagram contributes to various processes. In particular, when both baryonic external lines are on-shell the diagram contributes to most nucleon form factors, and the loop integral is a function of  $t \equiv q^2 = q_0^2 - \vec{q}^2$ .

If the baryon is represented by the Dirac field, the triangle diagram can be shown to have a branch-point singularity in the second Riemann sheet of  $t$ , an example of so-called anomalous threshold [14–17]. Reference [2] argued that the static-limit approximation is not aware of this second-sheet singularity, so a Lorentz-invariant treatment, or at least resummation of the recoil correction in HBChPT, is necessary.

However, from a more puristic point of view toward effective field theory (EFT), symmetries and degrees of freedom are the only constraints one must stand by. Along this line of thinking, if the anomalous threshold in the triangle diagram does turn out to account for important physics, one would like such an analytic structure to come out of the power counting, not the other way around.

We will show that a peculiarity of kinematics in the region centered around the two-pion cut  $t = 4m_\pi^2$ , where  $m_\pi$  is the pion mass, allows the baryon propagator to be unexpectedly close to its mass shell. This eventually leads to the loop integral being enhanced by  $\mathcal{O}(m_N/m_\pi)$ , compared with the standard ChPT counting. The enhancement of this sort resembles that of two-baryon

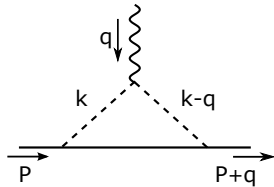


FIG. 1: The triangle diagram analyzed in the present paper. The solid (dashed) line represents the baryon (pion). The wavy line represents possible probes allowed by symmetries.

reducible diagrams [18], and it demands change of power counting just like in the two-baryon sector.

The manuscript is structured as follows. We first give a qualitative analysis on the diagram and point out the configurations of loop momenta that enhance the integral. Numerical results are shown in Sec. III, followed by a short summary in Sec. IV.

## II. INFRARED ENHANCEMENT

We choose the rest frame of the incoming baryon, so that its four-momentum is  $(m_N, \vec{0})$  where  $m_N$  is the baryon mass. The outgoing baryon has four-momentum  $(m_N + q_0, \vec{q})$ , with  $q_0$  and  $\vec{q}^2$  as functions of  $t$ :

$$q_0(t) = -\frac{t}{2m_N}, \quad \vec{q}^2(t) = t \left( -1 + \frac{t}{4m_N^2} \right). \quad (1)$$

In the physical region,  $q_0$  and  $\vec{q}^2$  are both positive real numbers; hence,  $0 > t > -4m_N^2$ . ChPT is expected to work in certain regions in the complex  $t$ -plane where  $|\vec{q}|$  is sufficiently small.

Note that the incoming baryon line can be taken to mean an outgoing antibaryon. If the antibaryon is on-shell  $(m_N, \vec{0})$ , the outgoing baryon is far off shell  $(-m_N + t/2m_N, \vec{q})$ , unless  $t$  is large and comparable to  $4m_N^2$ . Although both kinematic configurations—baryon form factor and baryon-antibaryon pair production—are very plausibly related by crossing symmetry, the latter is in principle out of the realm of ChPT.

The loop integral being investigated is given by

$$\gamma(t, m_\pi^2) \equiv i \int \frac{d^4 k}{(2\pi)^4} \frac{1}{k_0 - \frac{\vec{k}^2}{2m_N} + \dots + i\epsilon} \frac{1}{k^2 - m_\pi^2 + i\epsilon} \frac{1}{(k - q)^2 - m_\pi^2 + i\epsilon}, \quad (2)$$

where  $q$  and  $k$  label momenta as depicted in Fig. 1. We have so far used relativistic kinematics, even though the framework is not covariant. The only assumption we have made related to HBChPT is that the internal nucleon line always propagates forward, so the intermediate states do not include any baryon-antibaryon pairs.

Power counting à la Weinberg [19] tries to capture long-range physics represented by a loop diagram, by inspecting contributions from virtual three-momenta that push at least a subset of the propagators near their mass shell. When both pion propagators are on-shell,  $q$  and  $k$  satisfy the following equations:

$$k_0 = \sqrt{\vec{k}^2 + m_\pi^2}, \quad (3)$$

$$2\vec{k} \cdot \vec{q} - \vec{q}^2 - 2q_0 \sqrt{\vec{k}^2 + m_\pi^2} + q_0^2 = 0. \quad (4)$$

Since  $q_0 \simeq \vec{q}^2/2m_N$ ,  $\vec{k}$  is found to a first approximation to be collinear with  $\vec{q}$ , plus corrections in powers of  $1/m_N$ :

$$\vec{k} = \frac{\vec{q}}{2} + \mathcal{O}\left(\frac{\vec{q}^2}{m_N}\right), \quad (5)$$

and

$$k_0 = \sqrt{\vec{q}^2 + m_\pi^2} \left[ 1 + \mathcal{O}\left(\frac{\vec{q}^2}{m_N}\right) \right]. \quad (6)$$

Reasoning of the standard ChPT counting starts by assuming external three-momenta to be of the same order as the pion mass:  $Q \sim m_\pi$ , where we have used  $Q$  to denote generically the size of external three-momenta. Since the integral has dimension  $[mass]^{-1}$ , loop momenta with  $|\vec{k}| \gg Q$  do not contribute appreciably. Therefore, the meaningful integration volume of  $d^3k$  must be of order  $Q^3$ . In the physics region where  $\vec{q}^2 > 0$  and  $|\vec{q}| \sim m_\pi \sim Q$ , the volume of  $dk_0$  and  $k_0$  itself are too of order  $Q$ , according to Eq. (6). It follows immediately that the denominator of the baryon propagator is controlled by  $k_0 \sim Q$ , whereas the recoil correction  $\vec{k}^2/2m_N \sim Q^2/m_N$  is subleading. Therefore, the static limit is justified. With the baryon propagator and the pion propagators being counted respectively as  $Q^{-1}$  and  $Q^{-2}$ , we arrive at the standard counting that the loop integral (2) is of order  $Q^{-1}$ .

While the above argument covers the generic case of  $\vec{q}^2 \sim m_\pi^2$ , it, however, needs modification for peculiar cases defined by special values of  $\vec{q}^2$ . Pertinent to our concern in the present paper is the unphysical region where  $\vec{q}^2 = -4m_\pi^2 + \mathcal{O}(\xi^2 m_\pi^2)$ , with  $\xi \equiv m_\pi/m_N \ll 1$ ; therefore,  $t$  is near the two-pion cut  $t = 4m_\pi^2 + \mathcal{O}(\xi^2 m_\pi^2)$ . The condition (4) still holds, that the most important  $\vec{k}$ -modes are those around  $\vec{q}/2$ . Now that  $\vec{q}$  may take complex values,  $\vec{k}$  may too, i.e.,  $\vec{k}^2$  may be negative. So it is not surprising that there exists a small region of  $\vec{k}$  centered around  $\vec{q}/2$  in which the pion energy takes a value smaller than  $m_\pi$  by  $\mathcal{O}(m_\pi/m_N)$ :

$$|\vec{k} - \frac{\vec{q}}{2}| \sim \xi m_\pi, \quad k_0 \sim \sqrt{\vec{k}^2 + m_\pi^2} \sim \xi m_\pi, \quad \sqrt{(\vec{k} - \vec{q})^2 + m_\pi^2} \sim \xi m_\pi, \quad (7)$$

where we have used  $\vec{q}^2 \simeq -4m_\pi^2$ . Although this is a small region of  $k$ , with volume  $d^4k \sim (\xi m_\pi)^4$ , all of the three propagators have large values because they are very close to their mass shell. Especially,  $k_0$  in the denominator of the baryon propagator is now of order  $\xi m_\pi$ , so the recoil correction  $\vec{k}^2/2m_N \sim \xi m_\pi$  can no longer be considered subleading. It follows that the baryon propagator scales as  $\sim 1/(\xi m_\pi)$ , and the pion propagators  $\sim 1/(\xi m_\pi)^2$ .

Putting together these elements, we conclude that when  $t$  is within a small window around  $4m_\pi^2$ ,  $|t - 4m_\pi^2| \lesssim \xi^2 m_\pi^2$ , the loop integral is  $\sim (\xi m_\pi)^{-1}$ , enhanced by a factor of  $\xi^{-1}$  as opposed to

the aforementioned generic counting. Here the static limit is not a legitimate approximation taken by the baryon propagator: the leading recoil term  $-\vec{k}^2/2m_N$  must be retained in Eq. (2). The resummation of  $-\vec{k}^2/2m_N$  immediately reproduces the anomalous threshold [2], as it was rather anticipated.

### III. NUMERICS

#### A. Contours

We evaluate numerically the integral (2) with only the first recoil term kept in the baryon propagator:  $(k_0 - \vec{k}^2/2m_N)^{-1}$ . A Feynman parameter is first used to combine the pion propagators and then the following identity is used to incorporate the baryon propagator:

$$\frac{1}{ab} = 2 \int_0^\infty d\lambda \frac{1}{(a + 2\lambda b)^2}. \quad (8)$$

We then proceed by integrating out  $k$  after completing the square in  $k$ , eventually arriving at

$$\gamma(t, m_\pi^2) = \frac{1}{8\pi^2} \int_0^1 dx \int_0^\infty \frac{d\lambda}{\sqrt{1 + \frac{\lambda}{m_N}} x^2} \frac{1}{\left(q_0^2 - \frac{\vec{q}^2}{1 + \lambda/m_N}\right) - x \left(q_0^2 - \vec{q}^2 + 2\lambda q_0\right) + m_\pi^2 + \lambda^2}. \quad (9)$$

We wish to compare the above integral with its relativistic version:

$$\gamma_{rel}(t, m_\pi^2) = i \int \frac{d^4 k}{(2\pi)^4} \frac{2m_N}{k^2 - m_N^2 + i\epsilon} \frac{1}{k^2 - m_\pi^2 + i\epsilon} \frac{1}{(k - q)^2 - m_\pi^2 + i\epsilon}, \quad (10)$$

which has a well-known branch point at  $t = 4m_\pi^2$ . The comparison is facilitated if the branch point of  $\gamma(t, m_\pi^2)$  coincides that of  $\gamma_{rel}(t, m_\pi^2)$ . This can be achieved by retaining  $q_0(t)$  and  $\vec{q}^2(t)$  as defined in Eq. (1). If we had chosen to conform to nonrelativistic kinematics for the outgoing nucleon,  $q_0 = \vec{q}^2/2m_N$ ,  $q_0(t)$  and  $\vec{q}^2(t)$  would have been

$$q_0(t) = -\frac{t/2m_N}{2 \left(1 + \sqrt{1 + \frac{t}{m_N^2}}\right)}, \quad \vec{q}^2(t) = -\frac{t}{2 \left(1 + \sqrt{1 + \frac{t}{m_N^2}}\right)}. \quad (11)$$

However, the discrepancy between Eqs. (1) and (11) is not crucial for our qualitative statement regarding power counting.

To see how the branch point arises at  $t = 4m_\pi^2$ , we first notice that when  $\lambda = 0$  the integrand has two poles in the  $x$  plane, and they will pinch at  $x = 1/2$  when  $t = 4m_\pi^2$ . Because the pinching in the  $x$  plane happens at one of the end points of the  $\lambda$  integration, the corresponding singularity of the integrand is inevitable no matter how we deform the contours of  $\lambda$  and/or  $x$ . Therefore,  $\gamma(t, m_\pi^2)$  has a branch cut starting from  $t = 4m_\pi^2$ , running toward  $+\infty$  along the positive real axis.

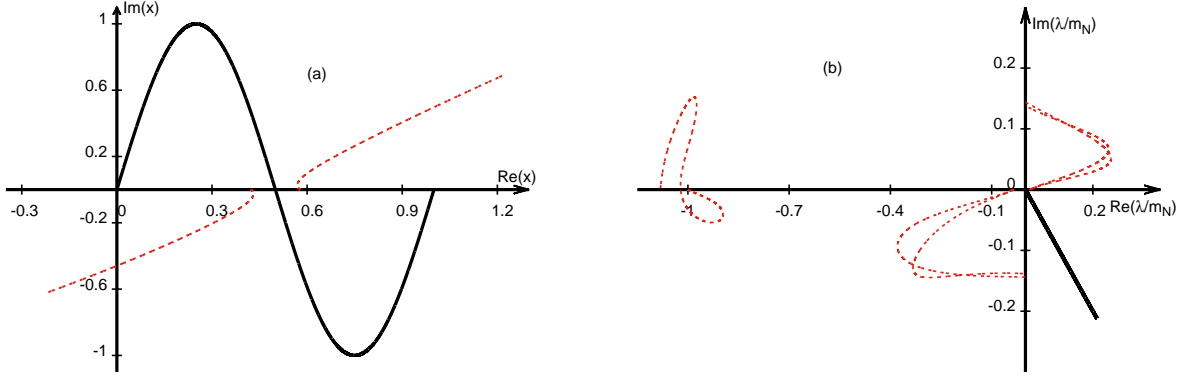


FIG. 2: The solid lines illustrate the contours of  $x$  and  $\lambda$  integrations, where  $y \equiv \lambda/m_N$ . The dashed lines represent the poles of the integrand in Eq. (9) when  $t = 4.1m_\pi^2$  (see the text for more detailed explanation).

For  $t > 4m_\pi^2$ , the contours in both  $x$  and  $\lambda$  planes need to be deformed so as not to be crossed by the poles of the integrand. The chosen contours are shown by the solid lines in Fig. 2. In particular, the  $\lambda$  contour is a straight line from the origin to infinity,  $45^\circ$  off the positive real axis. When  $\lambda$  takes a value on that contour, the integrand in Eq. (9) has corresponding poles in the  $x$  plane. The trajectories of these poles as  $\lambda$  moving along its contour are represented by the dashed lines in Fig. 2 (a), with  $t = 4.1m_\pi^2$ . A similar story goes to Fig. 2 (b), in which the  $\lambda$  contour is illustrated by the solid line and the poles associated with the  $x$  contour are marked out by the dashed lines. On a side note, there are other ways to evaluate the integral. For example, one can first calculate the imaginary part, i.e., the discontinuity along the branch cut, and then the real part by way of dispersion integral. In fact, this is the way integral (10) is evaluated.

The numerical results for the real and imaginary parts of  $\gamma(t, m_\pi^2)$  are plotted in Fig. 3, with  $m_\pi/m_N = 0.149$ — the ratio between the physical pion and nucleon masses. The solid lines correspond to evaluation of  $\gamma(t, m_\pi^2)$  according to Eq. 9. For comparison, we have also plotted the static-limit approximation (dashed), which diverges at  $t = 4m_\pi^2$ , and the relativistic results (dot-dashed) according to Eq. (2). The enhancement of  $\gamma(t, m_\pi^2)$  around  $t = 4m_\pi^2$  is clearly demonstrated by a peak in its real part and a rapid rise in its imaginary part.

The difference between the recoil and relativistic representations of the diagram is very small. This indicates that the higher-order recoil corrections like  $\vec{k}^4/8m_N^3$  are indeed subleading.

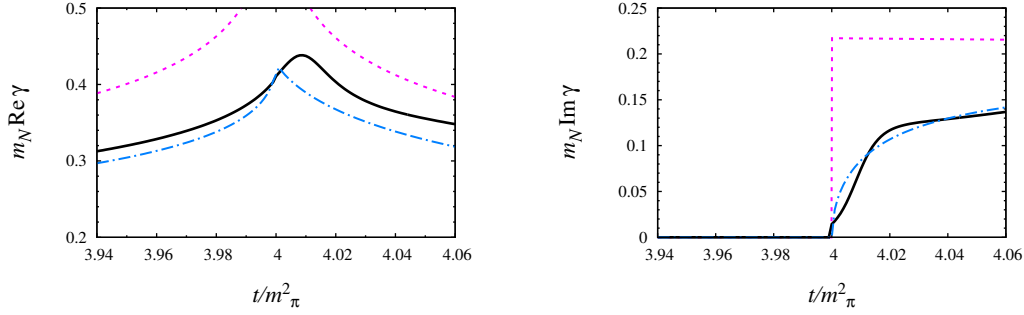


FIG. 3: Real and imaginary parts of  $\gamma(t, m_\pi^2)$  in neighborhood of  $t = 4m_\pi^2$ . The dashed, dot-dashed, and solid lines correspond respectively to calculations in the static limit, with the relativistic baryon propagator [Eq. (10)], and with the leading recoil term [Eq. (9)].

### B. Scaling of $\gamma(t, m_\pi^2)$

The infrared enhancement is essentially the statement that within a small window centered on  $t = 4m_\pi^2$ ,  $\gamma(t, m_\pi^2)$  scales like  $m_\pi^{-2}$ , rather than  $m_\pi^{-1}$ . The lack of analytic expression for  $\gamma(t, m_\pi^2)$  understandably obscures this point. We wish to demonstrate in this section how the scaling changes near  $t = 4m_\pi^2$ .

For this purpose, we rescale both low-energy mass scales— $t$  and  $m_\pi^2$ —by the same factor, while keeping the only large mass  $m_N$  fixed, and then look at how  $\gamma(t, m_\pi^2)$  varies with respect to the rescaling factor. More precisely, we define the following function to quantify the scaling behavior,

$$g(s; t/m_\pi^2) \equiv m_N \gamma(s^2 t, s^2 m_\pi^{*2}) , \quad (12)$$

with  $s = 1$  intentionally set up to correspond to the physical pion mass  $m_\pi^*$ :

$$g(1; t/m_\pi^2) = m_N \gamma(t, m_\pi^{*2}) . \quad (13)$$

When  $|t/m_\pi^2 - 4| \lesssim s^2 \xi_\star^2$ , where  $\xi_\star \equiv m_\pi^*/m_N = 0.149$ , we expect  $g \sim s^{-2}$ . When  $t/m_\pi^2$  is far outside of the enhancement window, which will always happen for a fixed  $t/m_\pi^2$  if  $s$  is small enough, the standard ChPT counting recovers and  $g \sim s^{-1}$ .

Figure 4 confirms the expected change of scaling. Shown in Fig. 4 is the log-log plot of  $g(s; t/m_\pi^2)$  versus  $s$ , for  $t/m_\pi^2 = 4.001$  and 7. When  $s$  is of  $\mathcal{O}(1)$ ,  $\text{Im}g(s; t/m_\pi^2 = 4.001)$  clearly scales as  $\sim s^{-2}$ , whereas the enhancement of the real part  $\text{Re}g(s; t/m_\pi^2 = 4.001)$  is milder, with a slope between  $-1$  and  $-2$ . Owing to its qualitative nature, however, it should not be utterly surprising that the power-counting analysis in Sec. II could not capture this difference between the real and imaginary parts of  $\gamma(t; m_\pi^2)$ . In the range of  $s$  we showed,  $t/m_\pi^2 = 7$  is always outside of the enhancement

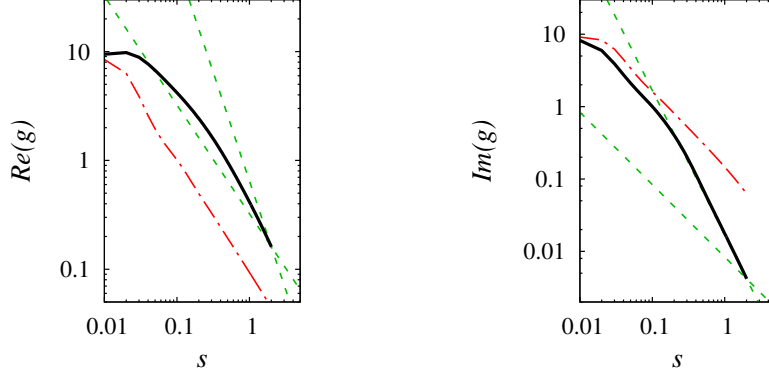


FIG. 4: The real and imaginary parts of  $g$  as functions of the scaling factor  $s$ , with various values for  $t/m_\pi^2$  [see the text for the definition of  $g(s; t/m_\pi^2)$ ]. The solid (dot-dashed) line has  $t/m_\pi^2 = 4.001$  ( $t/m_\pi^2 = 7$ ). The dashed lines are there to assist gauging the slope of the solid lines: The steeper dashed line has slope  $-2$ , and the other has slope  $-1$ .

window; therefore, both  $\text{Re}g(s; t/m_\pi^2 = 7)$  and  $\text{Im}g(s; t/m_\pi^2 = 7)$  show a slope of 1 in the log-log plots. When  $s$  is small enough, the enhancement window will be so narrow that for both values of  $t/m_\pi^2$ ,  $g$  is outside of it; therefore,  $g(s; t/m_\pi^2) \sim s^{-1}$ .

#### IV. SUMMARY AND CONCLUSION

We have shown an example of one-baryon processes with an infrared enhancement. More specifically, when  $t$  is inside a small window centered on the two-pion cut  $|t - 4m_\pi^2| \lesssim m_\pi^4/m_N^2$ , the triangle diagram is enhanced by a factor of  $m_N/m_\pi$ , compared with the standard ChPT counting. Similar to the two-baryon sector, the infrared enhancement calls for resumming baryon recoil corrections.

The main reason for this change of power counting is that the pion three-momenta in the loop can take complex values in the unphysical region, which in turn diminishes the pion energy flowing into the baryon internal line. Therefore, there exists an enhancement window in which the loop integral is dominated by modes that take all propagators to be close to their mass shell.

We have evaluated numerically the loop integral to demonstrate the enhancement near  $t = 4m_\pi^2$ . It was also found that there is very small discrepancy between the resummation of recoil terms and the fully relativistic calculation. More numerical evidence was shown to prove that the loop integral scales as  $Q^{-2}$  inside the enhancement window. This was done by rescaling small mass parameters  $\vec{q}$  and  $m_\pi$  by the same factor  $s$ , and investigating how the integral varies accordingly.



## Acknowledgments

BwL thanks the nuclear theory group at BeiHang University and the Institute for Nuclear Theory at the University of Washington for hospitality when part of the work was carried out there. This work was supported in part by the National Natural Science Foundation of China (NSFC) under Grant No. 11375120.

- 
- [1] E. E. Jenkins and A. V. Manohar, Phys. Lett. B **255**, 558 (1991).
  - [2] T. Becher and H. Leutwyler, Eur. Phys. J. C **9**, 643 (1999) [hep-ph/9901384].
  - [3] T. Fuchs, J. Gegelia, G. Japaridze, and S. Scherer, Phys. Rev. D **68**, 056005 (2003) [hep-ph/0302117].
  - [4] V. Pascalutsa and D. R. Phillips, Phys. Rev. C **67**, 055202 (2003) doi:10.1103/PhysRevC.67.055202 [nucl-th/0212024].
  - [5] V. Lensky, J. M. Alarcón, and V. Pascalutsa, Phys. Rev. C **90**, no. 5, 055202 (2014) [arXiv:1407.2574 [hep-ph]].
  - [6] J. M. Alarcón, J. Martin Camalich, and J. A. Oller, Phys. Rev. D **85**, 051503 (2012) [arXiv:1110.3797 [hep-ph]].
  - [7] Y. H. Chen, D. L. Yao, and H. Q. Zheng, Phys. Rev. D **87**, 054019 (2013) [arXiv:1212.1893 [hep-ph]].
  - [8] L. S. Geng, J. Martin Camalich, L. Alvarez-Ruso, and M. J. Vicente Vacas, Phys. Rev. Lett. **101**, 222002 (2008) [arXiv:0805.1419 [hep-ph]].
  - [9] J. Martin Camalich, L. S. Geng, and M. J. Vicente Vacas, Phys. Rev. D **82**, 074504 (2010) [arXiv:1003.1929 [hep-lat]].
  - [10] X.-L. Ren, L. S. Geng, J. Martin Camalich, J. Meng, and H. Toki, JHEP **1212**, 073 (2012) [arXiv:1209.3641 [nucl-th]].
  - [11] L. Geng, Front. Phys. China **8**, 328 (2013) [arXiv:1301.6815 [nucl-th]].
  - [12] J. Gasser, M. E. Sainio, and A. Svarc, Nucl. Phys. B **307**, 779 (1988).
  - [13] V. Bernard, N. Kaiser, and U. G. Meißner, Nucl. Phys. A **611**, 429 (1996) [hep-ph/9607428].
  - [14] Y. Nambu, Nuovo Cimento, **6**, 1064 (1957).
  - [15] L. D. Landau, Nucl. Phys. **13**, 181 (1959).
  - [16] M. Fowler, P. V. Landshoff, and R. W. Lardner, Nuovo Cimento, **17**, 936 (1960).
  - [17] R. J. Eden, P. V. Landshoff, D. I. Olive, and J. C. Polkinghorne, The analytic  $S$ -matrix, Cambridge University Press (1996).
  - [18] S. Weinberg, Nucl. Phys. B **363**, 3 (1991).
  - [19] S. Weinberg, Physica A **96**, 327 (1979).